Hindawi
Mathematical Problems in Engineering
Volume 2021, Article ID 6634762, 9 pages
https://doi.org/10.1155/2021/6634762

Research Article

Solitary Wave Diffraction with a Single and Two Vertical Circular Cylinders

Zouhair Hafsia,[1] Saliha Nouri,[1] Salah Mahmoud Boulaaras,[2] Ali Allahem,[3] Salem Alkhalaf,[4] and Aldo Munoz Vazquez[5]

[1]*Department of Physics, College of Science and Arts at ArRass, Qassim University, Buraydah, Saudi Arabia*
[2]*Department of Mathematics, College of Science and Arts at ArRass, Qassim University, Buraydah, Saudi Arabia*
[3]*Department of Mathematics, College of Science, Qassim University, Buraydah, Saudi Arabia*
[4]*Department of Computer Science, College of Science and Arts at ArRass, Qassim University, Buraydah, Saudi Arabia*
[5]*College of Engineering, Texas A&M University, Higher Education Center at McAllen, 6200 Tres Lagos Blvd, McAllen, TX 78504, USA*

Correspondence should be addressed to Ali Allahem; aallahem@qu.edu.sa

Received 12 December 2020; Revised 28 December 2020; Accepted 5 January 2021; Published 16 January 2021

Academic Editor: Sundarapandian Vaidyanathan

This study investigates the three-dimensional (3-D) solitary wave interaction with two cylinders in tandem and side-by-side arrangements for two wave heights. The solitary wave generation and propagation are predicted using the volume of fluid method (VOF) coupled with the NavierStokes transport equations. The PHOENICS code is used to solve these transport equations. The solitary wave generation based on the source line developed by Hafsia et al. (2009) is extended in three-dimensional wave flow and is firstly validated for solitary waves propagating on a flat bottom. The comparison between numerical results and analytical solution for small wave height $(H/h) = 0.1$ and 0.2 shows good agreements. The wave crest and the pseudo-wavelength are well reproduced. Excellent agreements were found in terms of maximum run-up and wave forces by comparison with the present model and analytical studies. The present model can be tested for the extreme solitary wave to extend its application to a more realistic case study as the solitary wave diffraction with an offshore oil platform.

1. Introduction

To ensure the safety of the offshore oil or airport platform, it is necessary to determine the interaction of the nonlinear waves with single or multiple cylinders structures. The main tasks of the wave structure interaction (WSI) problems are the prediction of the wave run-up, forces, breaking, and flow separation. The wave diffraction near multiple cylinders depended on the interference flow fields following the gap distance between the cylinders.

Different approaches are used to solve the WSI including experimental, analytical, or numerical methods. The interaction of a solitary wave (representing a real tsunami wave) with a single circular cylinder was studied experimentally by Yates and Wang [17] for weak and strong nonlinear waves. The development of a numerical wave tank (NWT) and its implementation on a computational fluid dynamics (CFD) code constitutes an alternative to the experiments (Cao and Wan [1], Windt et al. [2], and Ji et al. [3]). The NWT includes those based on full NavierStokes equations or the depth-average Boussinesq equations the simplified irrotational flow. The diffraction of monochromatic short-crested waves on a single vertical cylinder is studied by Zhu [4]. Based on the irrotational flow assumption, analytical solutions were proposed in this limiting assumption. Lin and Man [5] developed a nonlinear wave interaction around coastal structures by the extended Boussinesq equations of Nowogu. The computed results are compared to the full (3-D) NavierStokes results. Based on the Boussinesq model for wave generation and propagation, Zhao et al. [6] investigate numerically the solitary wave run-up around one, two, and four circular cylinders. The wave diffraction of the cnoidal

wave over two side-by-side or tandem arrangement is studied numerically by Wang and Ren [7] using a generalized Boussinesq model. Ning et al. [8] integrate the cut-cell method in a Boussinesq model to study the solitary wave diffraction in Cartesian grid cells.

The Boussinesq model has the advantage that it can be used for nonlinear wave transformation for large-scale problems. However, the nonlinear effects are not well reproduced due to average operation. Hence, the numerical solution of the complete NavierStokes equations in three-dimensional (3-D) is necessary. Xie et al. [9] used a cut-cell method in a fully (3-D) code to simulate solitary wave interaction with a vertical circular cylinder and a thin horizontal plate. The Smagorinsky subgrid-scale model was used to simulate the turbulence structure. The desired waves are generated by prescribing the analytical solutions at the inlet. The monochromatic wave diffraction through a rectangular cylinder was conducted using a (3-D) free surface model by Li et al. [10]. Zhi and Jie-Min [11] propose to generate a cnoidal wave through the specification of the incident wave characteristics at the inlet (velocity components induced by the desired wave). This three-dimensional model is used to predict the cnoidal wave run-up through a single bottom cylinder. Kriebel [12] presents a theoretical solution of the run-up around a circular cylinder due to regular and nonlinear monochromatic waves. The comparison of experimental and analytical solutions shows that the nonlinear nature of wave propagation has a large effect on wave run-up. A Large Eddy Simulation (LES) to predict turbulence structure is used by Mo et al. [12] for monochromatic wave flow interaction with a single circular cylinder. Kamath et al. [14] developed a full three-dimensional model to study the free surface displacements and wave forces on three and four vertical cylinders. Frantzis et al. [15] analyze numerically the reflection and transmission coefficients induced by a breakwater formed by a single row of vertical circular piles closely spaced. The free surface deformation is simulated using the (VOF) method, and the (LES) model was used to reproduce the small scales of turbulence.

The present study investigates numerically the interaction of solitary wave with a single and twin circular cylinder. The NWT was first validated for solitary wave propagating on a flat bottom and then used to simulate the wave force exerted on a single and twin circular cylinder in tandem and side-by-side arrangements. The source line used by Hafsia et al. [16] in two-dimensional (2-D) NavierStokes model has been extended to generate a nonlinear wave for a three-dimensional (3-D) model.

2. Mathematical Formulation

2.1. Computational Domain. Figure 1 represents the locations of the source line and the different grid regions to control the grid distributions through the computational domain. As shown in this figure, the incident solitary wave propagates along the x-direction and impacts one or two circular cylinders in two arrangements following the angle β: in tandem ($\beta = 0$) and side-by-side ($\beta = 90^{\circ}$). The ratio of the still water depth to cylinder radius is $(h/a) = 3$. For a given water depth $h = 0.2$ m, the cylinder ratio is $a = 0.067$ m. The two vertical cylinders are closely separated with $(G/2a) = 2$, where G is the gap distance between two cylinders (center to center). The wave forces are calculated for the tandem and side-by-side arrangements and for the following nondimensional wave heights: $(H/h) = 0.1$ and 0.2. Figure 2 presents the grid structure for two cylinders arranged in tandem with a refinement around the free surface and the circular cylinders. The two circular cylinders are represented using the cut-cell method in a Cartesian grid as shown by Figure 2(b). For all the cylinder arrangements, the grid number along the x-direction is taken equal to $N_x = 190$ and along the z-direction equal to $N_z = 94$. For a single cylinder and the tandem arrangement, the grid number along the y-direction: $N_y = 40$. However, for the side-by-side cylinders: $N_y = 60$. The same time step is adopted for all simulated cases $\Delta t = 0.01$ s.

2.2. Governing Transport Equations. The proposed (NWT) was based on the full three-dimensional (3-D) NavierStokes transport equations coupled to the volume of liquid (VOF) convective transport equation to reproduce the water wave interface. For unsteady flow and incompressible fluid, the mass and momentum conservation equations are written as follows:

The mass conservation equation:

$$\frac{\partial \rho}{\partial t} + \frac{\partial u_i}{\partial x_i} = 0. \tag{1}$$

The momentum transport equation:

$$\frac{\partial u_i}{\partial t} + u_j \frac{\partial u_i}{\partial x_j} = -\frac{1}{\rho}\frac{\partial p}{\partial x_i} + \frac{\partial}{\partial x_j}\left[\nu\left(\frac{\partial u_i}{\partial x_j} + \frac{\partial u_j}{\partial x_i}\right)\right] + g_i + s_{d,i}, \tag{2}$$

where x_i the Cartesian coordinates, u_i is the velocity components, ρ is the density of the mixture, p is the pressure, ν is the kinematic viscosity of the mixture, g is the acceleration due to gravity, and $s_{d,z}$ is a momentum source term added to the momentum equation along z-direction to avoid wave reflection at the open boundaries given by

$$s_{d,z} = \gamma\,(x)\, w. \tag{3}$$

where $\gamma(x)$ is a linear damping function and w is the velocity component along the z vertical direction.

2.3. Free Surface Capture. The air-water interface is modeled using the mixture model flow. If α_q denotes the volume fraction of the q th fluid in a cell, then

The density of the mixture is given by

$$\rho = \sum_{q=1}^{2} \rho_q\, \alpha_q. \tag{4}$$

where ρ_q is the density of the water when $(q = 1)$ and air when $(q = 2)$.

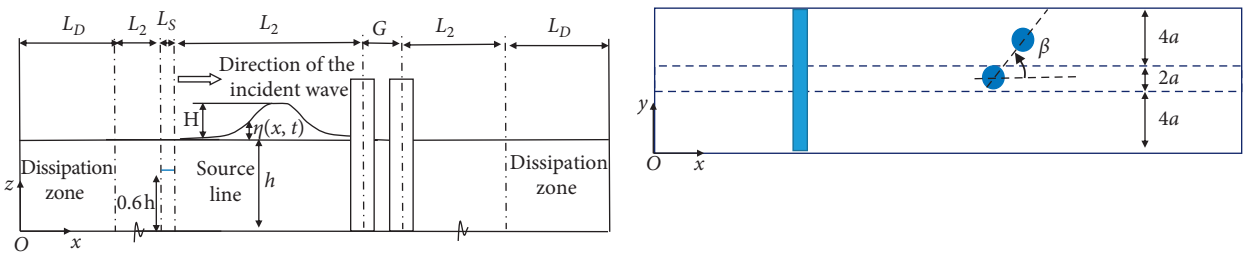

Figure 1: Grid regions of the computational domain and wave source line location: (a) side view; (b) top view.

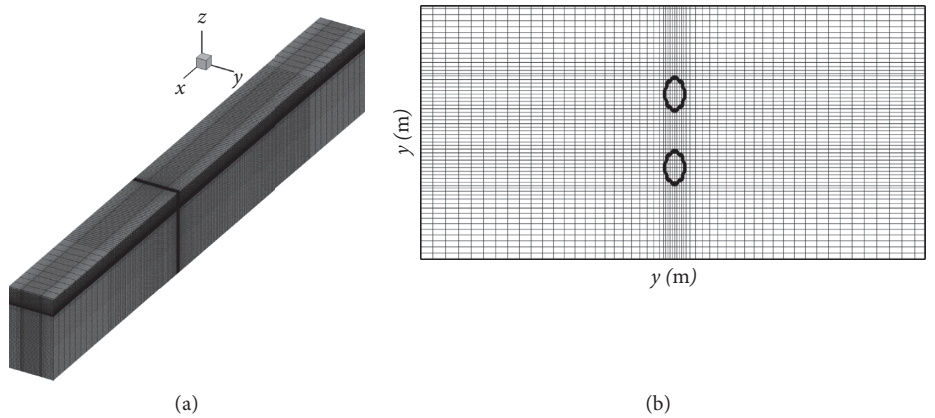

Figure 2: The grid of computational domain: (a) side view; (b) top view of the grid details around the side-by-side circular cylinders by the cut-cell method.

And, dynamic viscosity of the mixture is

$$\mu = \sum_{q=1}^{2} \mu_q \alpha_q. \tag{5}$$

where μ_q is the dynamic viscosity of the water if $(q = 1)$ and air when $(q = 2)$.

The volume fraction of fluid is determined by the following mass conservation equation for each phase:

$$\frac{\partial \alpha_q}{\partial t} + \frac{\partial\left(\alpha_q u_i\right)}{\partial x_i} = 0. \tag{6}$$

When $\alpha_q = 0$, the cell is occupied by air, $\alpha_q = 1$, the cell is occupied by water, and $0 < \alpha_q < 1$, the cell contains the interface (Hirt et al. [18]).

2.4. Wave Generation. The desired solitary wave was generated by an internal source inlet across a source line as proposed by Hafsia et al. [16]. The inlet vertical velocity is prescribed as a time-dependent inlet boundary condition:

$$w^I = \frac{2\, c\, \eta\left(x_s, t\right)}{L_s}, \tag{7}$$

where L_s is the length of the internal source line.

The wave celerity is given by Dominguez et al. [19]:

$$c = \sqrt{g\,(H + h)}. \tag{8}$$

The solitary wave surface elevation $\eta(x_s, t)$ is given by the following equation:

$$\eta = H \operatorname{sech}^2\left[k\,(x_s - c\,t)\right], \tag{9}$$

where H is the incident wave height and t is the time. The distance x_s permitting to have a negligible source at $t = 0$ s is determined by the following equation:

$$x_s = \frac{4h}{\sqrt{(H/h)}}. \tag{10}$$

The equivalent wave number k is

$$k = \sqrt{\frac{3\,H}{4h^2\,(H + h)}}. \tag{11}$$

Following this equivalent wave number, the pseudo-wave length can be determined by

$$L = \frac{2\pi}{k}. \tag{12}$$

Table 1 summarizes the wave parameters and the length of the source line L_s for the two considered wave height to water depth ratios. The length L_s and the position of the source line are determined by the calibration procedure as indicated by Hafsia et al. [16].

Table 1: Solitary wave parameters and the length of the source line.

	k (m^{-1})	c (m/s)	x_s (m)	L (m)	L_s (m)
$H/h = 0.1$	1.31	1.47	2.53	4.58	0.120
$H/h = 0.2$	1.77	1.53	1.79	3.24	0.072

2.5. Initial and Boundary Conditions. The following initial and boundaries conditions are adopted for the governing transport equations. The imposed initial condition is still water with a depth h. For the top boundary, the pressure P is set equal to the atmospheric pressure. Two dissipation zones are adopted at the open boundaries (Figure 1). At all the other boundaries of the computational domain, symmetric boundary conditions are imposed.

To solve this proposed model, we adopt the PHOENICS code (Parabolic Hyperbolic or Elliptic Numerical Integration Code Series). In this code, the SIMPLEST iterative algorithm is used to solve the pressure and velocity coupling in the NavierStokes equations (Artemov et al. [20]). The upwind scheme is used for nonlinear convection terms and an implicit formulation for the transient term. The VOF method is used to predict the interface between the water wave and air. For all the presented simulation results, the cut-cell within the PARSOL (PARtial SOLid) treatment is used to detect the solid-fluid interface which is not aligned with the Cartesian grid. The proposed three-dimensional wave generation method is implemented in the PHOENICS code.

3. Numerical Results

3.1. Wave Diffraction by a Single Circular Cylinder. The proposed wave generation method based on an internal source line is validated for two solitary waves having the nondimensional heights $H/h = 0.1$ and 0.2. The simulated results show that, before reaching the vertical cylinder, the wave profile is invariant in the transverse direction and can be represented by two-dimensional profiles in the center of the computational domain. Figure 3 represents the simulated wave profiles at the center of the computational domain before impacting the cylinder. For these two wave heights, the wave is not affected by the cylinder and the free surface profiles agree very well with the analytical one. The wave crests and the pseudo-wave lengths are in accordance with the analytical one. For $(H/h) = 0.1$, the wave is generated after $t = 3$ s. As the wave height increases, the solitary wave is completely generated more rapidly (after $t' = 2.3$ s).

In order to validate the cut-cell method, the maximum run-up is compared to the available literature. The maximum wave run-up is determined from the evolution of the solitary wave profiles along the centerline. In Figure 4, the solitary wave profiles are presented for different times around the maximum run-up which takes place at $t3 = 4.3$ s. For a nondimensional wave height, $H/h = 0.1$; the maximum wave run-up is equal to $R_{\max} = 0.0212$ m $= 1.060$ H which implies that the wave height increased by $(R_{\max} - H/H) * 100 = 6.0$ %. There is no significant difference between this value and the maximum run-up found by Domínguez et al. [19] that is equal to 1.065 for the same wave flow parameters. The maximum wave run-up increases when the wave height increases and is equal to $R_{\max} = 0.0466$ m $= 1.165$ H for $(H/h) = 0.2$ which implies that the wave height increased by 16.5 %. Following Domínguez et al. [19], the computed maximum run-up is 1.147 which is almost the same value given by the present study.

The evaluation of the wave forces exerted on the cylinder has great importance on the engineering applications and depends on the wave run-up R at the front of the stagnation point. The wave force $\vec{F}$ acting on the cylinder is computed by integrating the water pressure p and the normal component of the viscous stress tensor τ on the wetted surface of the cylinder S:

$$\vec{F} = \int_S (-\vec{n}\, p + \vec{n}.\tau)\mathrm{d}S, \tag{13}$$

where $\vec{n}$ is the normal unit vector pointing into the water.

The time histories of the computed wave force on the x-direction acting on an isolated cylinder are presented in Figure 5 for two different solitary wave heights. The peak of the in-line force becomes sharper when the solitary wave height increases. The computed forces are in good agreement with other numerical studies and the tested cut-cell method is validated.

3.2. Wave Diffraction by Two Circular Cylinders. Two vertical circular cylinders with the same radius are considered with different arrangements: in tandem ($\beta = 0$) and side-by-side ($\beta = 90^\circ$). The still water depth to the radius ratio is $h/a = 3$. The cylinder and the nondimensional gap distance is $G/2a = 2$. In order to explain the wave diffraction between the two cylinders, Figure 6 illustrates the perspective view of the free surface elevation at different instants for nondimensional wave height: $H/h = 0.2$. The free surface raised at the upstream side of the cylinder and decreases behind it. When the reflected diffracted wave propagates away of the upstream cylinder, the free surface elevation drops significantly. The maximum run-up with partial wave reflection propagating radially occurs at instant $t3 = 4.3$ s for $H/h = 0.1$ and at the instant $t'3 = 3.72$ s $H/h = 0.2$. This radial wave is also observed by Yates and Wang [17]. At the instant $t6 = 5.2$ s, the solitary wave almost passes through the cylinder and the portion of the wave nonblocked by the cylinder is diffracted around the cylinder.

In order to compare the wave forces, Figure 7 represents the evolution of the in-line wave forces on the two vertical cylinders and on the isolated cylinder. The maximum run-up on the upstream cylinder is almost the same as the isolated one. However, due to the wave field interference, the maximum run-up on the downstream cylinder is less than that on the upstream cylinder for tandem arrangement and

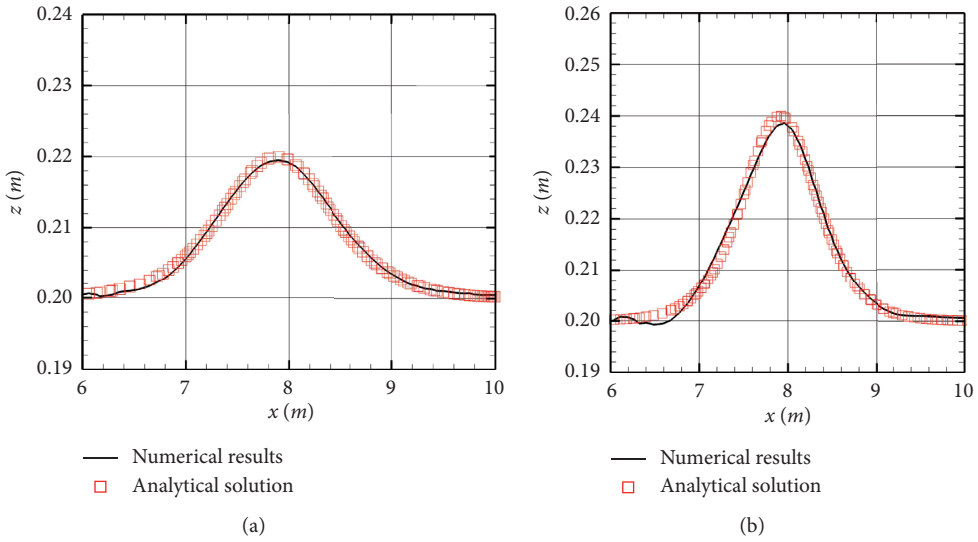

Figure 3: Comparison between the numerical and analytical free surface profiles at the centerline of computational domain: (a) $H/h = 0.1$ at $t = 3$ s and (b) $H/h = 0.2$ at t' = 2.3 s.

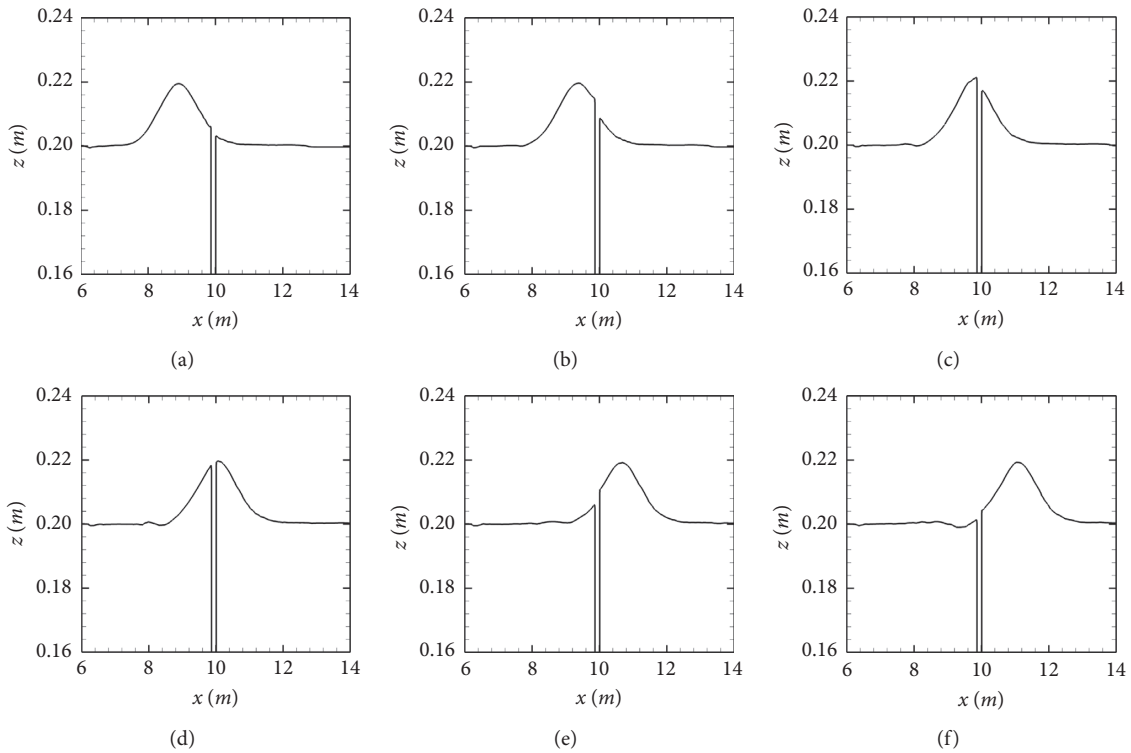

Figure 4: The wave run-up along the centerline of computational domain at different instants for $H/h = 0.1$: (a) $t_1 = 3.7$ s; (b) $t_2 = 4.0$ s; (c) $t_3 = 4.3$ s; (d) $t_4 = 4.5$ s; (e) $t_5 = 4.9$ s; (f) $t_6 = 5.2$ s.

$H/h = 0.1$. Following Yates and Wang [17], this interference effect is known as the shielding effect of the upstream cylinder on the downstream one. This mechanism induces the reduction of the in-line force on the downstream cylinder by 15 % compared to the force on the upstream cylinder (Table 2). The shielding effect is not observed for tandem arrangement and $H/h = 0.2$ where the in-line force on the downstream cylinder is greater than the upstream one (Table 3). For side-by-side arrangement, the wave force on the first cylinder is the same as that on the second cylinder for $H/h = 0.1$ and $H/h = 0.2$. The maximum force is observed at the same time for the two cylinders in side-by-side cylinders for the different wave heights. However, due to the gap distance, the maximum force for the downstream cylinder occurs after some time lag equal to 0.22 s.

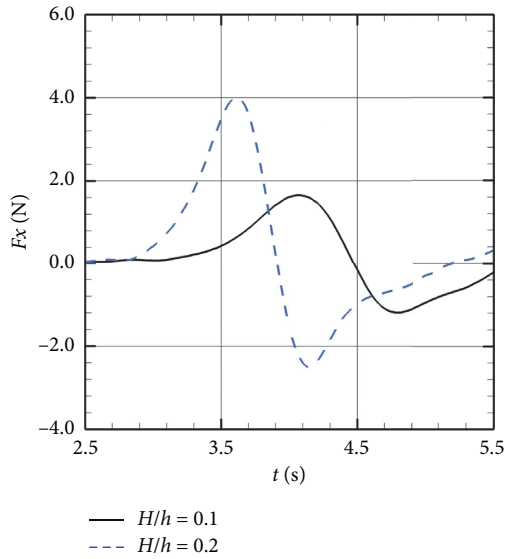

Figure 5: Time evolution of the in-line force on a single cylinder: (a) $H/h = 0.1$; (b) $H/h = 0.2$.

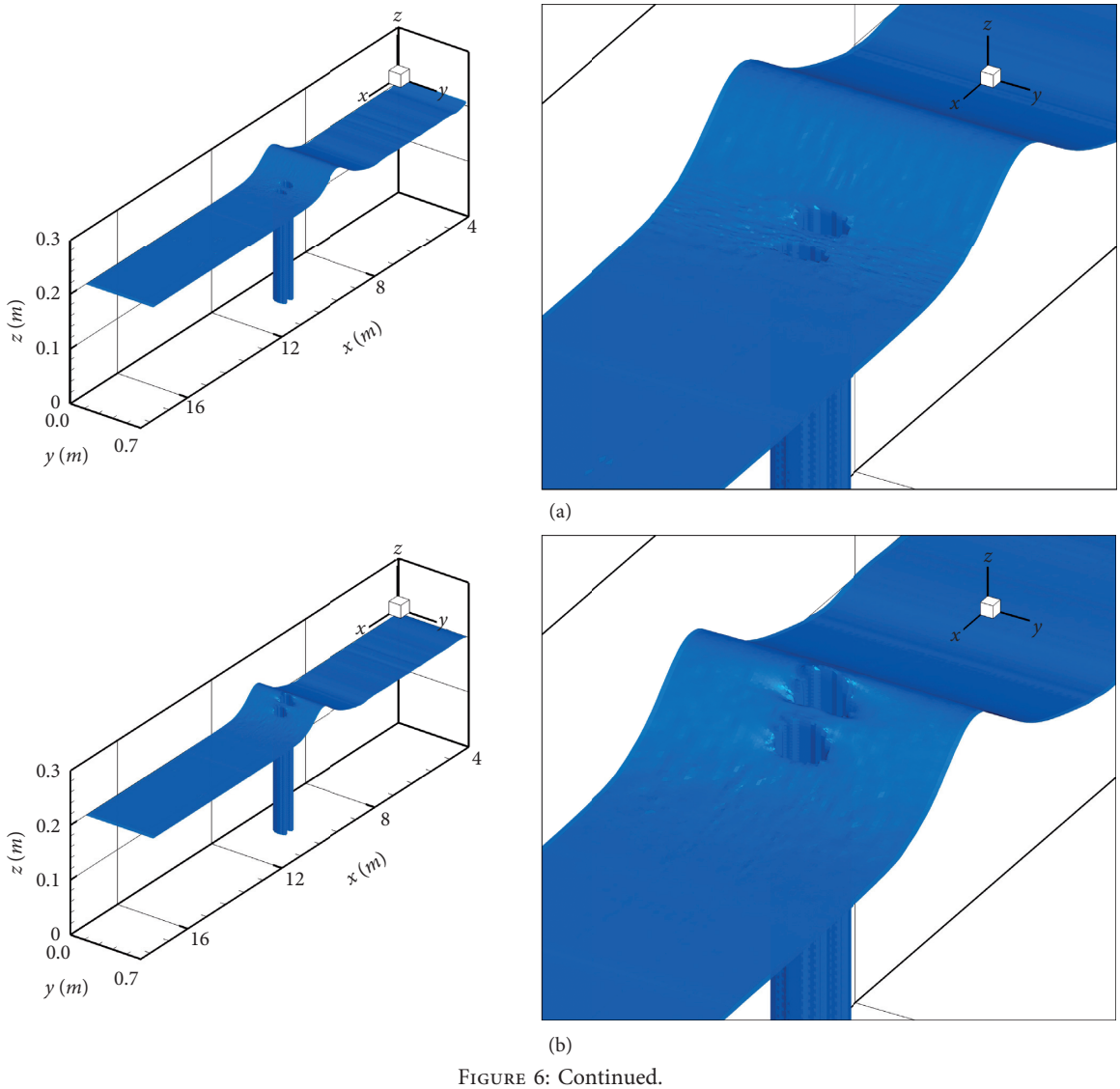

Figure 6: Continued.

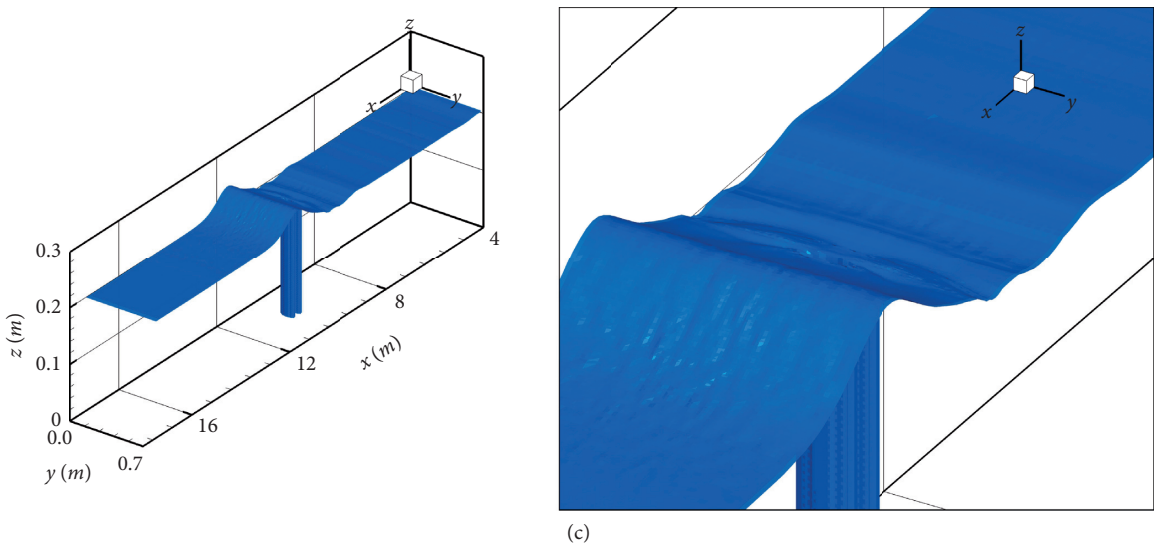

(c)

Figure 6: A three-dimensional free-surface elevation for two tandem circular cylinders ($\beta = 0^{\circ}$) at different times for $H/h = 0.2$: (a) $t_1 = 3.32$ s; (b) $t_2 = 3.72$ s; (c) $t_3 = 4.7$ s.

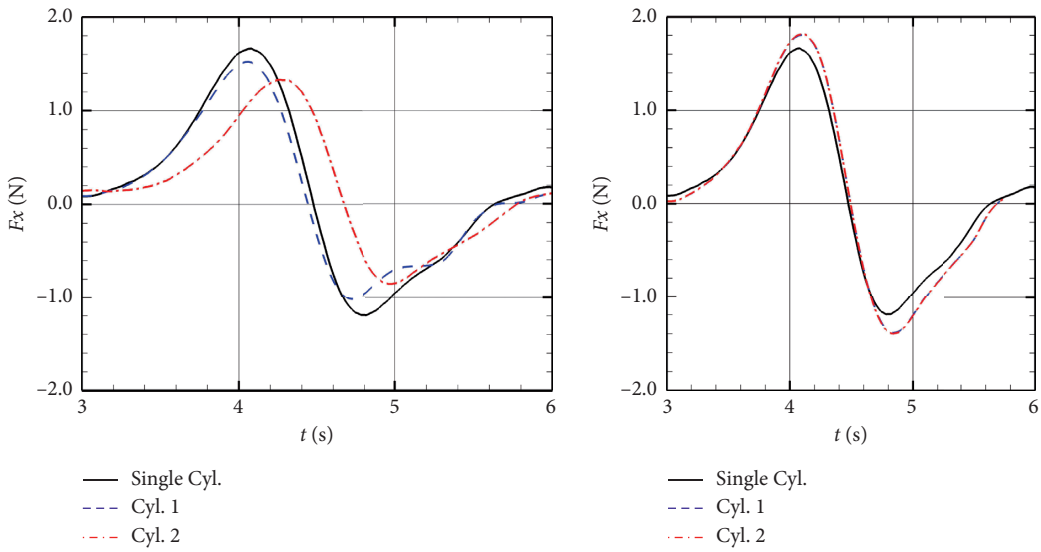

(a) (b)

Figure 7: Continued.

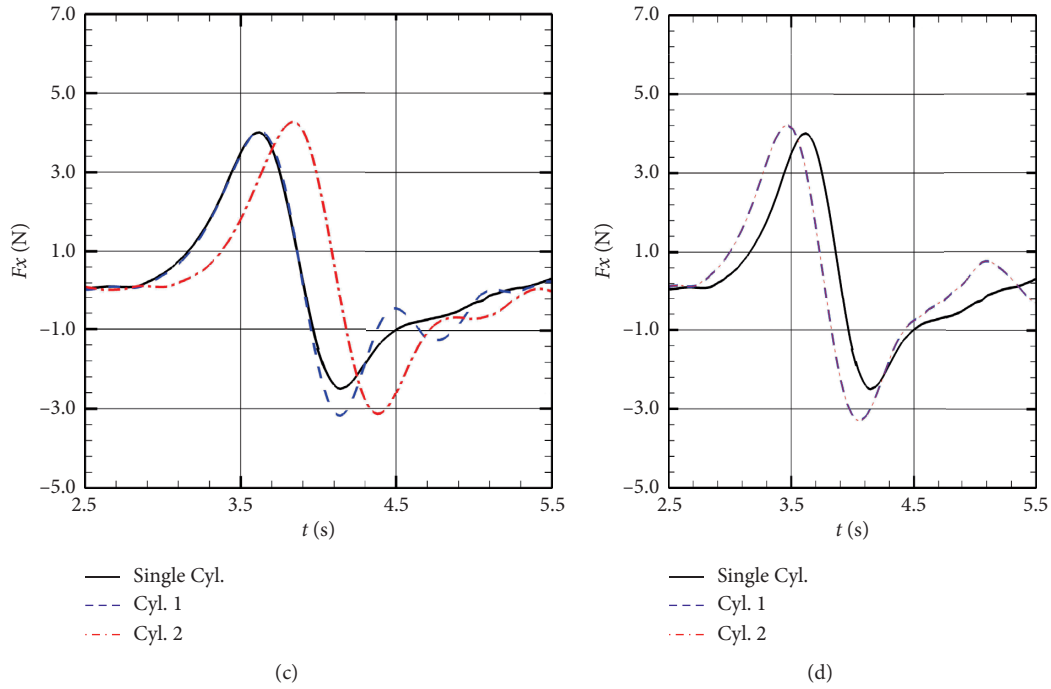

Figure 7: Time evolution of the in-line force on a single cylinder and two cylinders spaced by $G/a = 4$: (a) tandem circular cylinders ($\beta = 0^\circ$) for $H/h = 0.1$; (b) side-by-side circular cylinders ($\beta = 90^\circ$) for $H/h = 0.1$; (c) tandem circular cylinders ($\beta = 0^\circ$) for $H/h = 0.2$; (d) side-by-side circular cylinders ($\beta = 90^\circ$) for $H/h = 0.2$.

Table 2: Maximum and minimum in-line forces (N) for $H/h = 0.1$.

	Single cyl	Tandem arrangement ($\beta = 0$)		Side-by-side arrangement ($\beta = 90^\circ$)	
		Cyl 1	Cyl 2	Cyl 1	Cyl 2
$F_{x,\max}$	1.66	1.52	1.32	1.81	1.81
$F_{x,\min}$	−1.19	−1.02	−0.86	−1.39	−1.39

Table 3: Maximum and minimum in-line forces (N) for $H/h = 0.2$.

	Single cyl	Tandem arrangement ($\beta = 0$)		Side-by-side arrangement ($\beta = 90^\circ$)	
		Cyl 1	Cyl 2	Cyl 1	Cyl 2
$F_{x,\max}$	4.00	4.00	4.27	4.21	4.21
$F_{x,\min}$	−2.49	−3.17	−3.12	−3.29	−3.29

4. Conclusions

The proposed numerical wave tank (NWT) was validated for wave generation and wave diffraction with a single and two vertical circular cylinders for two solitary wave heights. All the simulated results are conducted in the Cartesian coordinates using the cut-cell method to represent the cylinder shape. Numerical results show that the solitary wave and the wave forces on the cylinder are well reproduced for a weak nonlinear wave. In the tandem arrangement and for $H/h = 0.1$, the shielding effect is observed. However, for $H/h = 0.2$, the in-line force for the downstream cylinder is greater than the upstream one. For the side-by-side arrangement, equally aligned, the in-line force for the two cylinders is the same. The diffracted wave affects this force compared to the single cylinder by some time lag.

The present model can be tested for the extreme solitary wave to extend its application to a more realistic case study as the solitary wave diffraction with an offshore oil platform.

Data Availability

No data were used to support the study.

Conflicts of Interest

The authors declare that they have no conflicts of interest regarding this study.

Acknowledgments

The third author would like to thank all the professors of the Mathematics Department at the University of Annaba in Algeria, especially his professors/scientists Pr. Mohamed Haiour, Pr. Ahmed-Salah Chibi, and Pr. Azzedine Benchettah for the important content of masters and PhD courses in pure and applied mathematics that he received during his studies. Moreover, he thanks them for the additional help they provided to him during office hours in their office about the few concepts/difficulties he had encountered, and he appreciates their talent and dedication for their postgraduate students currently and previously. The authors gratefully acknowledge Qassim University, represented by the Deanship of Scientific Research, on the financial support for this research under the number (10261-cos-2020-1-3-I) during the academic year 1442 AH/2020 AD.

References

[1] G. T. Yates and K. H. Wang, "Solitary wave scattering by a vertical cylinder: experimental study," in *Proceedings of the Fourth International Offshore and Polar Engineering Conference*, Osaka, Japan, April 1994.

[2] H. Cao and D. Wan, "Benchmark computations of wave run-up on single cylinder and four cylinders by naoe-FOAM-SJTU solver," *Applied Ocean Research*, vol. 65, p. 327, 2017.

[3] C. Windt, J. Davidson, E. J. Ransley et al., "Validation of a CFD-based numerical wave tank model for the power production assessment of the wavestar ocean wave energy converter," *Renewable Energy*, vol. 146, 2020.

[4] Q. Ji, Y. Wang, and G. Zhang, "Numerical study of solitary wave interaction with a submerged semicircular cylinder," *Mathematical Problems in Engineering*, vol. 2019, pp. 1–15, 2019.

[5] S. Zhu, "Diffraction of short-crested waves around a circular cylinder," *Ocean Engineering*, vol. 20, no. 4, 1993.

[6] P. Lin and C. Man, "A staggered-grid numerical algorithm for the extended Boussinesq equations," *Applied Mathematical Modelling*, vol. 31, no. 2, pp. 349–368, 2007.

[7] M. Zhao, L. Cheng, and B. Teng, "Numerical simulation of solitary wave scattering by a circular cylinder array," *Ocean Engineering*, vol. 34, no. 3-4, pp. 489–499, 2007.

[8] K.-H. Wang and X. Ren, "Interactions of cnoidal waves with cylinder arrays," *Ocean Engineering*, vol. 26, pp. 1–20, 1999.

[9] D. Z. Ning, J. Zang, Q. Liang, P. H. Taylor, and A. G. L. Borthwick, "Boussinesq cut-cell model for non-linear wave interaction with coastal structures," *International Journal for Numerical Methods in Fluids*, vol. 57, no. 10, pp. 1459–1483, 2008.

[10] Z. Xie, T. Stoesser, S. Yan, Q. Ma, and P. Lin, "A Cartesian cut-cell based multiphase flow model for large-eddy simulation of three-dimensional wave-structure interaction," *Computers & Fluids*, vol. 213, no. 15, pp. 1–17, 2020.

[11] Y. S. Li, S.-X. Liu, Y.-X. Yu, and G.-Z. Lai, "Numerical modeling of Boussinesq equations by finite element method," *Coastal Engineering*, vol. 37, no. 2, pp. 97–122, 1999.

[12] D. Zhi and Z. Jie-Min, "Numerical modeling of wave evolution and runup in shallow water," *Journal of Hydrodynamics*, vol. 21, no. 6, pp. 731–738, 2009.

[13] D. L. Kriebel, "Non-linear wave interaction with a vertical cylinder. part II: wave run-up," *Ocean Engineering*, vol. 19, no. 1, pp. 475–499, 1992.

[14] W. Mo, K. Irschik, H. Oumeraci, and P. L.-F. Liu, "A 3D numerical model for computing non-breaking wave forces on slender piles," *Journal of Engineering Mathematics*, vol. 58, no. 1-4, pp. 19–30, 2007.

[15] A. Kamath, H. Bihs, M. A. Chella, and O. A. Arntsen, "Upstream-cylinder and downstream-cylinder influence on the hydrodynamics of a four-cylinder group," *Journal of Waterway, Port, Coastal, and Ocean Engineering*, vol. 142, no. 4, Article ID 04016002, 2016.

[16] C. Frantzis, D. G. E. Grigoriadis, and A. A. Dimas, "Numerical study of solitary waves past slotted breakwaters with a single row of vertical piles: wave processes and flow behavior," *Ocean Engineering*, vol. 211, no. 1, pp. 1–21, 2020.

[17] Z. Hafsia, M. B. Hadj, H. Lamloumi, and K. Maalel, "Internal inlet for wave generation and absorption treatment," *Coastal Engineering*, vol. 56, no. 9, pp. 951–959, 2009.

[18] C. W. Hirt and B. D. Nichols, "Volume of fluid (VOF) method for the dynamics of free boundaries," *Journal of Computational Physics*, vol. 39, no. 1, pp. 201–225, 1981.

[19] J. M. Domínguez, C. Altomare, J. Gonzalez-Caoa, and P. Lomonaco, "Towards a more complete tool for coastal engineering: solitary wave generation, propagation and breaking in an SPH-based model," *Coastal Engineering Journal*, vol. 61, pp. 1–15, 2019.

[20] V. Artemov, S. B. Beale, G. de Vahl Davis et al., "A tribute to D.B. Spalding and his contributions in science and engineering," *International Journal of Heat and Mass Transfer*, vol. 52, no. 17-18, pp. 3884–3905, 2009.